

Magnetism in one-dimensional quantum dot arrays

K. Kärkkäinen, M. Koskinen, S.M. Reimann* and M. Manninen

*Nanoscience Center, Department of Physics,
FIN-40014 University of Jyväskylä, Finland and*

**Mathematical Physics, Lund Institute of Technology, SE-22100 Lund, Sweden*

(Dated: January 7, 2022)

Abstract

We employ the density functional Kohn-Sham method in the local spin-density approximation to study the electronic structure and magnetism of quasi one-dimensional periodic arrays of few-electron quantum dots. At small values of the lattice constant, the single dots overlap, forming a non-magnetic quantum wire with nearly homogenous density. As the confinement perpendicular to the wire is increased, i.e. as the wire is squeezed to become more one-dimensional, it undergoes a spin-Peierls transition. Magnetism sets in as the quantum dots are placed further apart. It is determined by the electronic shell filling of the individual quantum dots. At larger values of the lattice constant, the band structure for odd numbers of electrons per dot indicates that the array could support spin-polarized transport and therefore act as a spin filter.

PACS numbers: 73.21.-b, 75.75.+a, 85.35.Be, 85.75.-d

I. INTRODUCTION

Quantum dots or “artificial atoms”, as they are frequently called, confine a few electrons on a small conduction electron island, built in (or from) a semiconductor heterostructure. Being finite-sized fermion systems, quantum dots can show strong shell effects which determine their physical properties. Just like for atoms, quantum dots with closed shells are particularly stable, implying “noble” structures for certain numbers of electrons in the dot. Following Hund’s rules, at half-filling of a shell, orbital degeneracy can lead to spin alignment. This was discovered first for small vertical quantum dot samples with circular-parabolic shape by Tarucha *et al.*¹. The experimental findings were later theoretically confirmed by electronic structure calculations using mean field methods as well as quantum Monte Carlo techniques or even a numerical diagonalization of the full many-body Hamiltonian (see Reimann and Manninen² for a review).

Experimentally, few-electron quantum dot structures where the shell effects on magnetism could be observed, are challenging to fabricate. One example where spontaneous magnetism has been found, are one-dimensional quantum point contact constrictions formed in a gate-patterned heterostructure^{3,4,5}. The intrinsic magnetic properties of these nanostructures have drawn much attention recently due to their potential applicability in spintronics devices⁶. Quantum point contacts⁷ and single quantum dots^{8,9} were found to have spin filtering capabilities, with a possibility to serve for either generating or detecting spin-polarized currents.

Arranging many quantum dots in a lattice, one can build artificial crystals with designed band structure^{10,11} which can be manipulated for example by tuning the inter-dot coupling and the number of confined electrons in the single quantum dots. The dot lattice does not suffer from structural deformations, which has the advantage that it can be designed freely without having to consider lattice instabilities¹².

Fabrication of a quasi one-dimensional artificial crystal consisting of a sequence of a few quantum dots was suggested by Kouwenhoven *et al.*¹⁰ already in 1990. They observed oscillations in the conductance as a function of gate voltage, arising from the mini-band structure in the periodic crystal. Small dots in well-ordered lattices could be synthesized by self-organized growth¹³. A particularly interesting artificial lattice structure is the Kagome lattice, due to the possibility of flat-band ferromagnetism^{12,14,15,16,17}. Shiraishi *et al.*¹⁴ have pointed at the importance of these structures for fast processing and high-density storage of information.

For square lattices, Koskinen *et al.*¹⁸ showed within the density-functional scheme that few-electron quantum dot lattices have a rich magnetic phase diagram, depending on the lattice constant and electron number. Related observations have been made also within the

Hubbard model^{12,19,20}.

In this paper, we investigate the electronic and magnetic properties of quasi one-dimensional quantum dot arrays. We suggest that such linear quantum dot chains could, in fact, lead to single-spin conductivity.

In our model the single quantum dot confinement is provided by a rigid Gaussian-shaped background charge distribution. At the single dot centers, this potential is approximately parabolic. The band structure and the magnetic properties depend on the lattice constant, a , and the number of electrons per dot, N . Here, conductivity of the dot chain is only considered by observing whether there is a band gap at the Fermi-level or not, which allows a qualitative understanding.

At small values of the lattice constant, the single dots overlap, forming a non-magnetic quantum wire with nearly homogenous density. As the confinement perpendicular to the wire is increased, i.e. the wire is squeezed to become more one-dimensional, the ground state is a spin density wave caused by a spin-Peierls transition^{21,22,23}. Magnetism sets on as the lattice constant is increased. It is determined by the shell structure of the individual dots: the arrays are non-magnetic insulators for closed single-dot shells at $N = 2$ and 6. At half-filled shell ($N = 4$) the spin of the dot is determined by Hund's rule and the array is an antiferromagnetic insulator. Ferromagnetism is observed both at the beginning and the end of a shell (here $N = 3, 5$). The spin-up and spin-down bands are separated by the exchange splitting. At sufficiently large lattice constant a one observes a gap between these bands. In this case the current would be carried by a single spin only, acting as a spin filter.

II. THE COMPUTATIONAL METHOD

In order to model the one-dimensional quantum dot array, we consider interacting electrons moving in two dimensions in a rigid periodic background charge distribution $e\rho_B$. The background charge number per unit cell is chosen to match the electronic charge of the unit cell in order to ensure overall charge neutrality. We employ the Kohn-Sham method with periodic boundary conditions. The Kohn-Sham orbitals are of Bloch form $\psi_{n\mathbf{k}\sigma}(\mathbf{r}) = \exp(i\mathbf{k} \cdot \mathbf{r})u_{n\mathbf{k}\sigma}(\mathbf{r})$, where n labels the band, $\sigma = (\downarrow, \uparrow)$ is the spin index and the wave vector \mathbf{k} is confined into the first Brillouin zone. The periodic functions $u_{n\mathbf{k}\sigma}(\mathbf{r})$ satisfy the Bloch-Kohn-Sham equations

$$-\frac{\hbar^2}{2m^*}(\nabla + i\mathbf{k})^2 u_{n\mathbf{k}\sigma}(\mathbf{r}) + v_{eff}^\sigma(\mathbf{r})u_{n\mathbf{k}\sigma}(\mathbf{r}) = \varepsilon_{n\mathbf{k}\sigma}u_{n\mathbf{k}\sigma}(\mathbf{r}) \quad (1)$$

where the periodic effective potential is

$$v_{eff}^\sigma(\mathbf{r}) = \int \frac{e^2(\rho(\mathbf{r}') - \rho_B(\mathbf{r}'))}{4\pi\epsilon_0\epsilon|\mathbf{r} - \mathbf{r}'|}d\mathbf{r}' + v_{xc}^\sigma[\rho(\mathbf{r}), \xi(\mathbf{r})], \quad (2)$$

ρ is the electron density and $\xi = (\rho_{\uparrow} - \rho_{\downarrow})/\rho$ is the polarization. In the local spin-density approximation we use the generalized²⁴ Tanatar-Ceperley²⁵ parameterization for the polarization-dependent exchange-correlation potential $v_{xc}^{\sigma}[\rho(\mathbf{r}), \xi(\mathbf{r})]$. In the band structure calculation, the functions $u_{n\mathbf{k}\sigma}(\mathbf{r})$ are expanded in a basis with 11×11 plane waves. For one-dimensional systems, the wave vector reduces to wave number for which we chose an equidistant 19-point mesh in the first Brillouin zone. The self-consistent iterations were started with anti-ferromagnetic and ferromagnetic initial potentials. Small random perturbations were added to the initial guesses in order to avoid convergence into saddle points of the potential surface. In addition, we use an artificial temperature to allow fractional occupation numbers for nearly degenerate states at the Fermi level. We noted that by decreasing the temperature the amplitudes of the spin-density and the average spin per dot become somewhat higher for small lattice constants. Nevertheless, we must emphasize that the temperature is low enough not to affect the ground-state. The statistical occupations merely help occupying degenerate levels to ensure convergence. We use effective atomic units with Hartree $\text{Ha} = m^*e^4/\hbar^3(4\pi\epsilon_0\epsilon)^2$ for energy and the Bohr radius $a_B^* = \hbar^2 4\pi\epsilon_0\epsilon/m^*e^2$ for length, where m^* is the effective mass and ϵ the dielectric constant of the semiconductor material in question.

III. MAGNETISM IN A 1D QUANTUM DOT ARRAY

Studying magnetism in a one-dimensional array, the simplest geometry to choose for the unit cell is a rectangle with two quantum dots per cell. These dots lie in a row along the x axis of the cell, one in the center and one crossing periodically the edge of the cell. The confining potential is modeled by a periodic positive background charge distribution described by a sum of Gaussians centered at lattice sites $\mathbf{R} = a(n_x, 0)$, $n_x = 0, 1, 2, \dots$,

$$\rho_B(\mathbf{r}) = \sum_{\mathbf{R}} \rho_d(\mathbf{r} - \mathbf{R}); \quad \rho_d(\mathbf{r}) = \frac{1}{\pi r_s^2} \exp(-r^2/Nr_s^2), \quad (3)$$

where $\mathbf{r} = (x, y)$ is a two-dimensional position vector. A single Gaussian carries positive charge Ne with density $1/\pi r_s^2$ at the center. The parameter r_s determines the average electron density at the center of the dot. Throughout this paper we use the value $r_s = 2 a_B^*$ which is close to the equilibrium density of the two-dimensional electron gas. The bottom of the confining potential provided by the background charge distribution is harmonic to a good approximation. Since there are two quantum dots in the unit cell, the electronic levels are split into bonding and anti-bonding bands. As a consequence, for both spins there are two 1s-bands, four p-bands, six 2s1d-bands and so on. In a one-dimensional quantum dot array one can have a smooth transition from the tight-binding description to the nearly-free

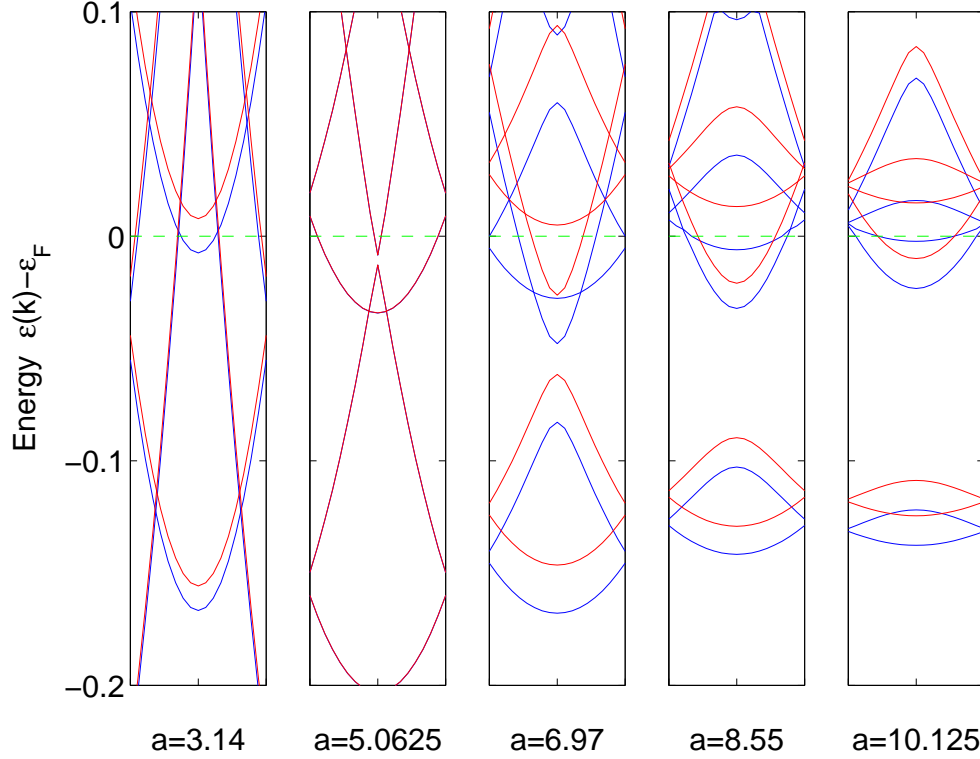


FIG. 1: Lowest bands at selected values of the lattice constant a for a quantum dot array with three electrons per quantum dot (in atomic units, see text). The spin-down bands are plotted in blue color, and spin-up bands are plotted in red. The dashed green line indicates the Fermi-level fixed at zero energy.

electron picture simply by varying the lattice constant a .

Figure 1 shows the bands for $N = 3$ with different inter-dot separations. Spin-up and spin-down bands are plotted in red and blue color, respectively, and the Fermi-level is fixed at zero energy. The spin degeneracy is lifted by the exchange splitting. For very large values of the lattice constant a , the electron densities of the single dots hardly overlap, and the dots are isolated.

The energies of ferromagnetic and anti-ferromagnetic solutions are nearly degenerate as the local approximation is unable to distinguish between them. Furthermore, the bands are flat with band gap energies approximately equal to the single dot level spacings. Even though the Fermi energy stays inside a band, the dot array becomes an insulator due to a diminished hopping probability between the single dots in this limit.

By decreasing a , i.e. by bringing the quantum dots closer to one another, the band dispersion increases. The bands corresponding to some specific quantum dot level are bunched and the bunches are separated by energy gaps, which is demonstrated in figure 1 for lattice

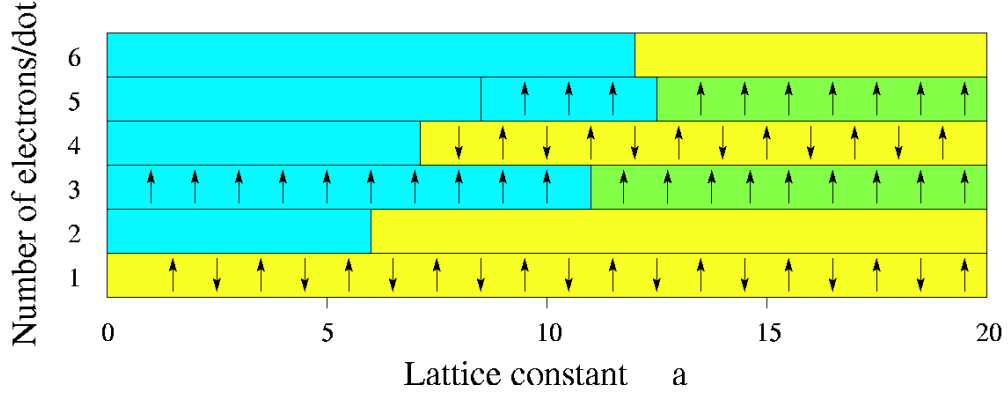


FIG. 2: Magnetism in a linear chain of quantum dots as a function of the number of electrons per dot, and the lattice constant. Blue color corresponds to the conducting, yellow to the insulating phase. Green indicates the phase where only one spin is conductive.

constant $a = 10.125 a_B^*$. By decreasing a further, the band gaps close. For sufficiently small a the quantum dots overlap strongly, which leads to an essentially homogenous quantum wire with a Gaussian cross-section. In this nearly-free limit the transverse motion separates from the longitudinal one. Consequently, the transverse states are quantized by the Gaussian-shaped well, while the longitudinal states remain “free” with parabolic dispersion. This is reflected in the band structure, showing nearly equidistant sub-band parabolae where the n th sub-band for a given k corresponds to a Kohn-Sham-Bloch orbital with $n - 1$ nodes in the transverse direction. We note also that the higher bands have parabolic dispersion at longer inter-dot separations than the lower ones due to the longer spatial extent of high-energy orbitals. From figure 1 we note that the second transverse sub-band is occupied at $a = 5.0625 a_B^*$ while at $a = 3.14 a_B^*$ the Fermi-level reaches the third sub-band. Having now also the higher transverse modes occupied, the quantum dot chain becomes *quasi* one-dimensional.

Figure 2 shows the magnetism of the quasi-1D quantum dot array as a function of electron number per quantum dot and lattice constant a . The colors indicate the regions where the array is conducting (blue) or insulating (yellow). The green bars indicate regions where the Fermi-level resides solely on a single spin band. The arrows indicate the spin arrangement in the array.

For a single electron per quantum dot, $N = 1$ only the bonding s-band is filled. Due to the exchange splitting of the single dot levels, the bonding and anti-bonding bands are separated by an energy gap and the array shows anti-ferromagnetic order. Figure 3 shows that the average spin per dot, calculated by integrating the spin density over a single dot, drops gradually from $1/2$ to 0 as the lattice constant is decreased. The band gap and thus the

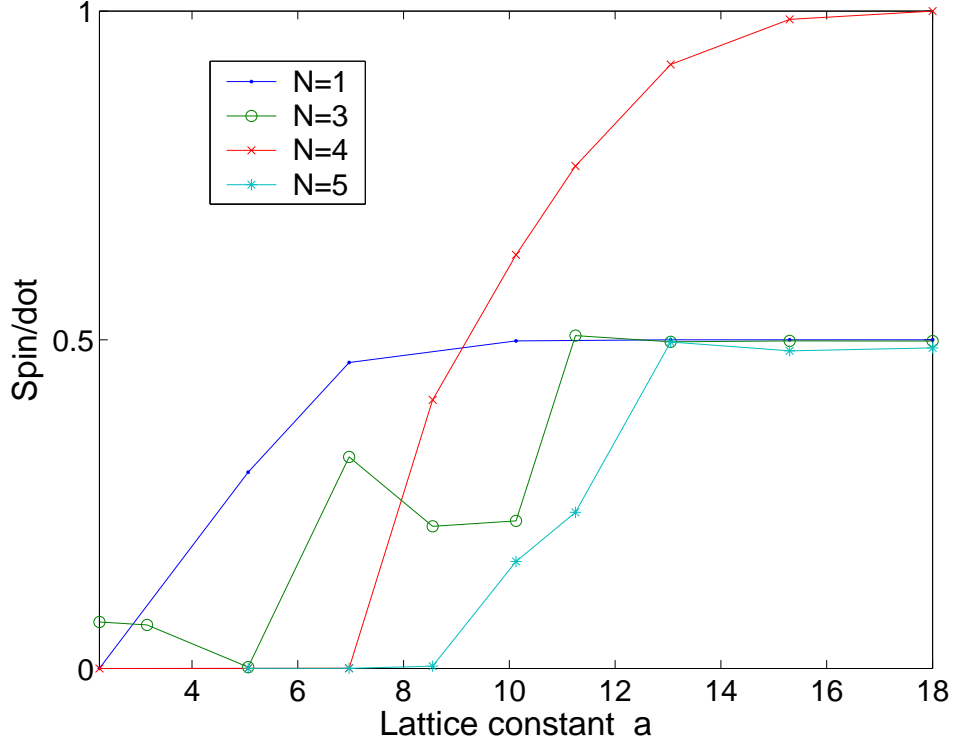


FIG. 3: Spin per dot for $N=1,3,4$ and 5 as a function of lattice constant.

antiferromagnetism persists down to very small values of the lattice constant. At the closed shell $N = 2$ the bonding and anti-bonding 1s-bands are filled leading to a non-magnetic insulator. The transition from a tightly bound insulator to a nearly free metal occurs at the lattice constant $a \approx 6 a_B^*$, when the gap between the 1s- and p-bands closes up.

Next, the p-bands are occupied. There are two degenerate p-orbitals for a single dot giving rise to two bonding bands and two anti-bonding bands for both the spins as shown in figure 4. The orbitals with density lobes oriented along the wire yield higher dispersion than the ones perpendicular to it. For $N = 3$ there is one p-electron per quantum dot, which triggers ferromagnetism. An example of the total electron and spin densities is shown in Fig. 5. The levels with majority spin are lower than the ones with minority spin as a result of the exchange splitting of the energy bands. The density in the array increases as the dots are brought closer. Consequently, the kinetic energy becomes the dominant contribution to the total energy. From figure 1 we note that at $a = 5.0625 a_B^*$ the dispersion is parabolic and the spin degeneracy is restored. However, there is a competition between the kinetic and exchange energies. It turned out that at $a = 3.14 a_B^*$ a small spin-splitting is re-gained.

Since the Fermi-level is bound to the p-band region, the array with three electrons per dot remains conductive at all lattice constants. Figure 4 shows that the bands of the minority spin are pushed up in energy by exchange splitting. As a consequence, just before the

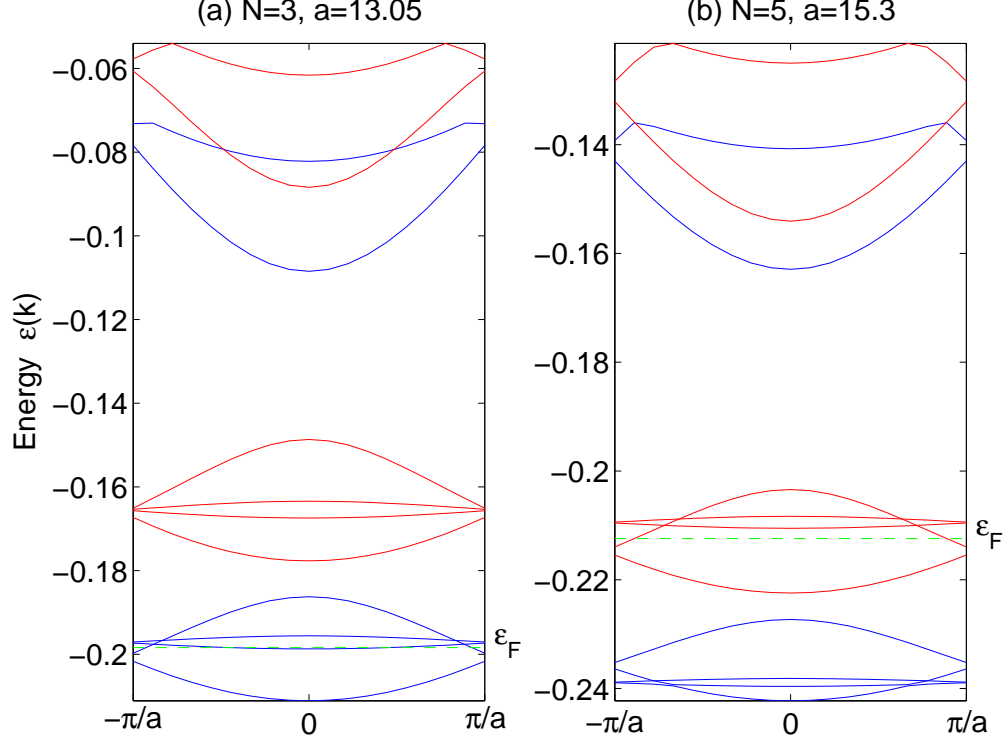


FIG. 4: 1p-bands and lowest 2s1d-bands for (a) $N = 3$ at $a = 13.05 a_B^*$ and (b) $N = 5$ at $a = 15.3 a_B^*$. The blue lines are the spin-down bands, the red lines the spin-up bands. The dashed green line indicates the Fermi level. The spin-up and spin-down bands are separated by a gap which leads to single-spin conductivity.

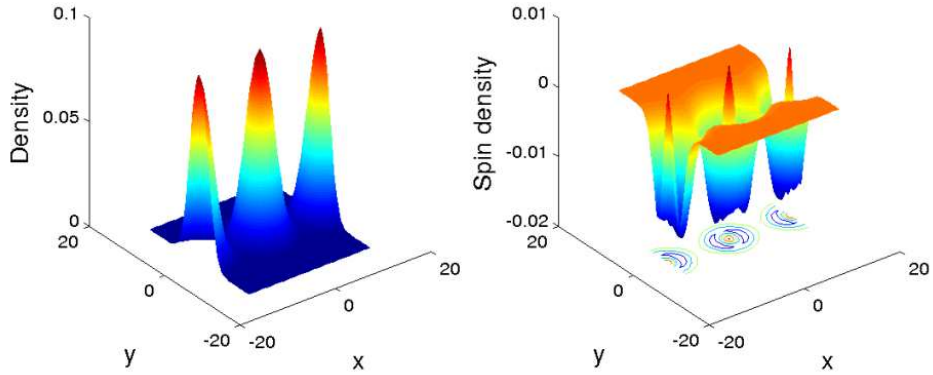


FIG. 5: Total density and spin density for $N = 3$ at lattice constant $13.05 a_B^*$.

insulating phase, when the bandwidths are relatively narrow, the Fermi-level for the minority spin lies in the band-gap but the majority spin remains conductive. A similar behavior is found in the case of $N = 5$ since there are three p-electrons and the shell is almost filled. However, this time the minority spin is conductive because the levels with fewer electrons are pushed to higher energies. The spin-dependent conductivity might open an intriguing opportunity to use the linear quantum dot chain as a spin filter.

At half-filled p-shell ($N = 4$) Hund's rule leads to maximized spin in an isolated quantum dot. Indeed, the spin per dot for $N = 4$ is at its maximum (1.0) at lattice constant $a \approx 18 a_B^*$ and it decreases gradually with a as the spin densities "spill" into the other dots. Due to Hund's rule and the exchange-splitting, the anti-ferromagnetic ordering of spins is favored. Since a gap is formed at the Fermi-surface, the array is insulating until a transition to a nearly homogenous wire occurs. Finally for $N = 6$, the p-shell is filled and the linear quantum dot chain remains non-magnetic at all values of a .

IV. SPIN-PEIERLS TRANSITION IN A HOMOGENOUS QUANTUM WIRE

At small values of the lattice constant a the quantum dots overlap significantly, forming a homogenous quantum wire with a Gaussian cross-section. Let us look at this limit more closely. Consider a quantum wire with a Gaussian cross-section closed in a rectangular unit cell. The background charge distribution is chosen to be

$$\rho_B(x, y) = \frac{1}{2r_s^{1D}} \frac{1}{\sqrt{2\pi}\alpha} \exp\left(-\frac{y^2}{2\alpha^2}\right), \quad (4)$$

where r_s^{1D} is the one-dimensional density parameter. The wire lies along the x -axis and its width is measured by the full width at half maximum $2\sqrt{2\ln 2}\alpha$. Since there is no definite lattice parameter for the wire, the length L of the unit cell is chosen such that ρ_B integrates to the desired charge Ne , thus we have $L = 2r_s^{1D}N$. We have chosen four electrons in the unit cell ($N = 4$) and fixed $r_s^{1D} = 2 a_B^*$. In addition, we define parameter $C_{1D} = 2r_s^{1D}/\alpha$ to describe the ratio of the average inter-electron separation and the width of the wire: with increasing C_{1D} the wire becomes narrower. Consequently, the energies of the higher transverse modes are pushed up in energy.

Figure 6 shows band structures of homogenous quantum wires for selected widths. For $C_{1D} = 2$, the dispersion is parabolic and the Fermi-level lies close to the second transverse sub-band. In this case the wire shows no magnetism. Antiferromagnetism sets on at $C_{1D} = 4$, as the spin-Peierls transition occurs. The ground state is a spin density wave with wave length of $L/2 = r_s^{1D}N = 8 a_B^*$. The spin-Peierls transition opens a gap at the Fermi-level and turns the wire into an insulator. The amplitude of the spin density wave increases with increasing C_{1D} .

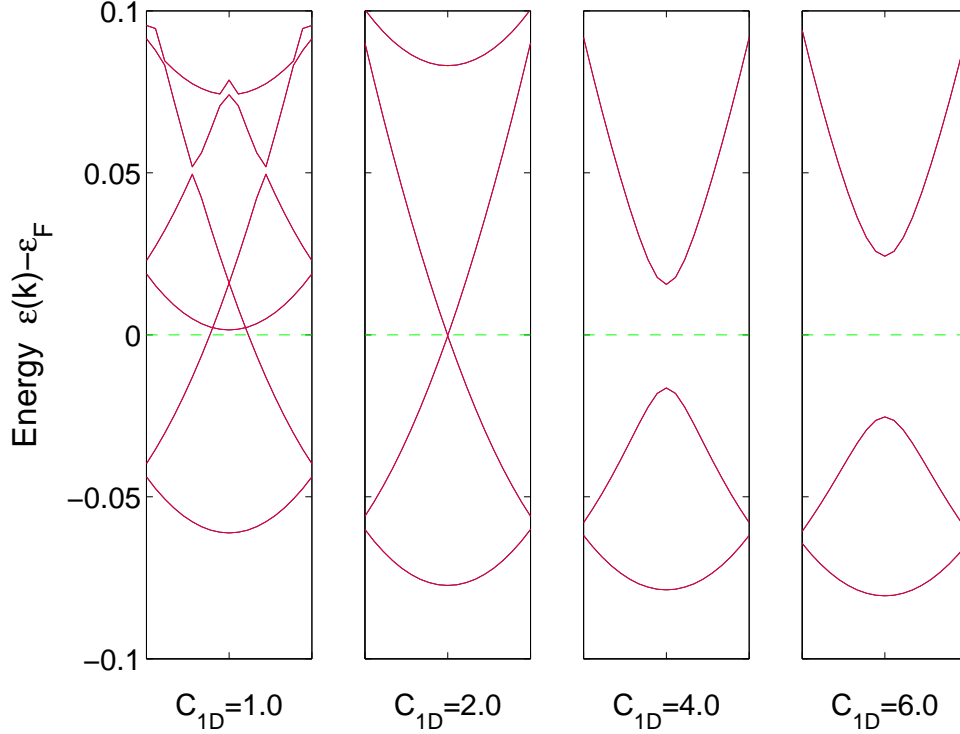


FIG. 6: Lowest bands at selected values of width parameter C_{1D} for a quantum wire with four electrons per unit cell. The dashed green line indicates the Fermi-level fixed at zero energy.

V. SUMMARY

We studied the electronic and magnetic properties of one-dimensional arrays of few-electron quantum dots. The spin per dot, and thus the magnetism of the array, depends on the shell filling of the individual dots and the inter-dot coupling. Furthermore the band structure of chains with open-shell dots suggests that conductivity could become spin dependent at suitable values of the lattice constant.

Acknowledgments

We thank M. Borgh for helpful discussions. This work was financially supported by the Academy of Finland, the European Community project ULTRA-1D (NMP4-CT-2003-505457), the Swedish Research Council and the Swedish Foundation for Strategic Research.

- ¹ S. Tarucha, D.G. Austing, T. Honda, R.J. van der Haage, and L.P. Kouwenhoven, Phys. Rev. Lett. **77**, 3613 (1996).
- ² S.M. Reimann and M. Manninen, Rev. Mod. Phys. **74**, 1283 (2002).
- ³ K.J. Thomas, J.T. Nicholls, M.Y. Simmons, M. Pepper, D.R. Mace, and D.A. Ritchie, Phys. Rev. Lett. **77**, 135 (1996).
- ⁴ K. S. Pyshkin, C. J. B. Ford, R. H. Harrell, M. Pepper, E. H. Linfield, and D. A. Ritchie, Phys. Rev. B **62**, 15 842 (2000).
- ⁵ A. Heyman, I. l Yakimenko and K-F Berggren, Nanotechnology **15**, 143 (2004).
- ⁶ I. Žutić, J. Fabian and S. Das Sarma, Rev. Mod. Phys. **76**, 323 (2004).
- ⁷ R.M. Potok, J.A. Folk, C.M. Marcus, and V. Umansky, Phys. Rev. Lett. **89**, 266602 (2002).
- ⁸ J. A. Folk, R.M. Potok, C.M. Marcus, and V. Umansky, Science **299**, 679 (2003).
- ⁹ J. Fransson, I. Sandalov and O. Eriksson, J. Phys.: Condens. Matter **16**, L249 (2004).
- ¹⁰ L.P. Kouwenhoven, F.W.J. Hekking, B.J. van Wees, C.J.P.M. Harmans, C.E. Timmering, and C.T. Foxon, Phys. Rev. Lett. **65**, 361 (1990).
- ¹¹ R.J. Haug, J.M. Hong, and K.Y. Lee, Surf. Sci. **263**, 415 (1992).
- ¹² H. Tamura, K. Shiraishi, T. Kimura, and H. Takayanagi, Phys. Rev. B **65**, 085324 (2002).
- ¹³ J. Temmyo, E. Kuramochi, T. Tamamura, and H. Kamada, J. Cryst. Growth **195**, 516 (1998).
- ¹⁴ K. Siraishi, H. Tamura, and H. Takayanagi, Appl. Phys. Lett. **78**, 3702 (2001).
- ¹⁵ T. Kimura, H. Tamura, K. Shiraishi, H. Takayanagi, Phys. Rev. B **65**, 081307(R) (2002).
- ¹⁶ T. Kimura, H. Tamura, K. Kuroki, K. Shiraishi, H. Takayanagi, and R. Arita, Phys. Rev. B **66**, 132508 (2002).
- ¹⁷ P. Mohan, F. Nakajima, M. Akabori, J. Motohisa, T. Fukui, Appl. Phys. Lett. **83**, 689 (2003).
- ¹⁸ M. Koskinen, S. M. Reimann, and M. Manninen, Phys. Rev. Lett. **90**, 066802-1 (2003).
- ¹⁹ H. Chen, J. Wu, Z.-Q. Li, and Y. Kawazoe, Phys. Rev. B **55**, 1578 (1997).
- ²⁰ P. Koskinen, L. Sapienza and M. Manninen, Physica Scripta **68**, 74 (2003).
- ²¹ R. Peierls, *Quantum Theory of Solids* (Clarendon Press, Oxford, 1955).
- ²² J. R. Hook and H. E. Hall, *Solid State Physics* (Wiley, Chichester, 1991).
- ²³ S.M. Reimann, M. Koskinen, and M. Manninen, Phys. Rev. B **59**, 1613 (1999).
- ²⁴ M. Koskinen, M. Manninen and S.M. Reimann, Phys. Rev. Lett. **79**, 1389 (1997).
- ²⁵ B. Tanatar and D.M. Ceperley, Phys. Rev. B **39**, 5005 (1989).